Weak Pinning and Long-Range Anticorrelated Motion of Phase Boundaries in Driven Diffusive Systems

Sören Schweers,[1,*] David F. Locher,[1,2,†] Gunter M. Schütz,[3,‡] and Philipp Maass[1,§]
[1]Universität Osnabrück, Fachbereich Mathematik/Informatik/Physik, Institut für Physik, Barbarastraße 7, D-49076 Osnabrück, Germany
[2]Institute for Quantum Information, RWTH Aachen University, 52056 Aachen, Germany
[3]Departamento de Matemática, Instituto Superior Técnico, Universidade de Lisboa, Avenida Rovisco Pais 1, 1049-001 Lisbon, Portugal

(Received 18 October 2023; accepted 19 March 2024; published 16 April 2024)

We show that domain walls separating coexisting extremal current phases in driven diffusive systems exhibit complex stochastic dynamics with a subdiffusive temporal growth of position fluctuations due to long-range anticorrelated current fluctuations and a weak pinning at long times. This weak pinning manifests itself in a saturated width of the domain wall position fluctuations that increases sublinearly with the system size. As a function of time t and system size L, the width $w(t,L)$ has a scaling behavior $w(t,L) = L^{3/4} f(t/L^{9/4})$, with $f(u)$ constant for $u \gg 1$ and $f(u) \sim u^{1/3}$ for $u \ll 1$. An Orstein-Uhlenbeck process with long-range anticorrelated noise is shown to capture this scaling behavior. The exponent $9/4$ is a new dynamical exponent for relaxation processes in driven diffusive systems.

DOI: 10.1103/PhysRevLett.132.167101

Driven diffusive systems of interacting particles exhibit a large variety of nonequilibrium structures [1,2]. Fundamental aspects of them, such as the occurrence of phase boundaries even in one dimension or the appearance of dynamical critical behavior in the celebrated Kardar-Parisi-Zhang (KPZ) universality class [3,4], can be understood from the study of driven lattice gas (DLG) models [2,5–14]. These models have found numerous applications, ranging from microscale processes, such as ionic, colloidal, and molecular transport through narrow channels [15–17], ribosome translation along mRNA strands [18–23], cargo transport and motility of molecular motors [24–27], or interface growth [28–30] to macroscopic processes subject to randomness like vehicular traffic [9,31–35].

In DLGs with boundaries open to particle reservoirs, phase transitions between nonequilibrium steady states occur even in one dimension [36,37]. They manifest themselves in a singular behavior of the bulk particle density ρ_B as a function of the control parameters, which are the rates of particle injection from and ejection into the reservoirs. By applying bulk-adapted couplings [38–40], all possible nonequilibrium phases can be inferred from the principle of extremal current [41]: for particle densities ρ_L and ρ_R of reservoirs at the left and right boundary, the bulk density ρ_B in the system's interior is

$$\rho_B = \begin{cases} \underset{\rho_L \le \rho \le \rho_R}{\operatorname{argmin}} \{j_B(\rho)\}, & \rho_L \le \rho_R, \\ \underset{\rho_R \le \rho \le \rho_L}{\operatorname{argmax}} \{j_B(\rho)\}, & \rho_R \le \rho_L, \end{cases} \tag{1}$$

where $j_B(\rho)$ is the current in the nonequilibrium steady state (NESS) of a closed system, as, e.g., obtained for periodic boundary conditions. Equation (1) implies that if $j_B(\rho)$ has a local extremum at some ρ_{ext}, an extremal current phase with $\rho_B = \rho_{\text{ext}}$ must occur. These phases are particularly interesting because they are determined by the intrinsic dynamics: the bulk density is controlled but not induced by the coupling to reservoirs.

The dynamics of phase boundaries between coexisting nonequilibrium phases with different ρ_B have been studied in the prototype DLG [42–44], the asymmetric simple exclusion process (ASEP) and variants of it, where particle interactions are solely due to site exclusion, i.e., a lattice site can be occupied by at most one particle. In the standard ASEP, two boundary-induced phases with $\rho_B = \rho_L$ and $\rho_B = \rho_R$ coexist at $\rho_L = 1 - \rho_R \le 1/2$ [45,46] and the domain wall (DW) separating them performs a random walk with reflecting boundaries. The universal dynamical critical behavior of open DLGs is thus widely considered to be well understood: Density fluctuations relax with the dynamical exponent $z = 3/2$ of the KPZ universality class [36], while the diffusive dynamical critical exponent $z = 2$ governs the domain wall fluctuations [42].

In this Letter we unravel the dynamical behavior of phase boundaries between coexisting *extremal* current phases which appear in the presence of two local maxima (minima) at densities $\rho_1 \neq \rho_2$ with $j_B(\rho_1) = j_B(\rho_2)$. A representative model having a current-density relation with two degenerate local maxima is the ASEP with repulsive nearest neighbor-interactions between particles [39–41,47].

We show that the DW separating the two maximal current phases exhibits a fascinating dynamical and localization behavior: the fluctuations of its position have a width w increasing subdiffusively with time due to long-range anticorrelations of local current fluctuations, $w \sim t^{1/3}$. At long times, w saturates at a value w_{sat} increasing sublinearly with the system size L, $w_{\mathrm{sat}} \sim L^{3/4}$. This implies that the DW in the saturated regime appears randomly over an infinite region in the thermodynamic limit, while it covers a zero fraction of the system, as the relative saturated width $w_{\mathrm{sat}}/L \sim L^{-1/4}$ goes to zero for $L \to \infty$. We refer to this localization behavior as weak pinning of the DW. As a function of t and L, $w(t, L)$ obeys the scaling law

$$w(t, L) = L^{\alpha} f(t/L^{z}), \tag{2}$$

where $\alpha = 3/4$, $z = 9/4$, and $f(u) \sim u^{\beta}$ with $\beta = 1/3$ for $u \ll 1$, and $f(u) \sim \text{const}$ for $u \gg 1$. A Langevin equation is set up, which describes the scaling behavior of $w(t, L)$. The stochastic DW motion provides an intriguing example for anomalous subdiffusion generated by long-range autocorrelated noise, and the unexpected dynamic exponent $9/4$ is intimately connected to the weak pinning effect.

Figure 1(a) illustrates the totally asymmetric simple exclusion process (TASEP) with nearest-neighbor interactions and open boundaries. The particles perform unidirectional jumps between neighboring lattice sites i, $i = 1, \ldots, L$, where the jump rate $\Gamma_i(n_{i-1}, n_{i+2})$ from a site i to a vacant site $(i+1)$ is given by the Glauber rate

$$\Gamma_i(n_{i-1}, n_{i+2}) = \frac{\nu}{\exp[V(n_{i+2} - n_{i-1})] + 1}. \tag{3}$$

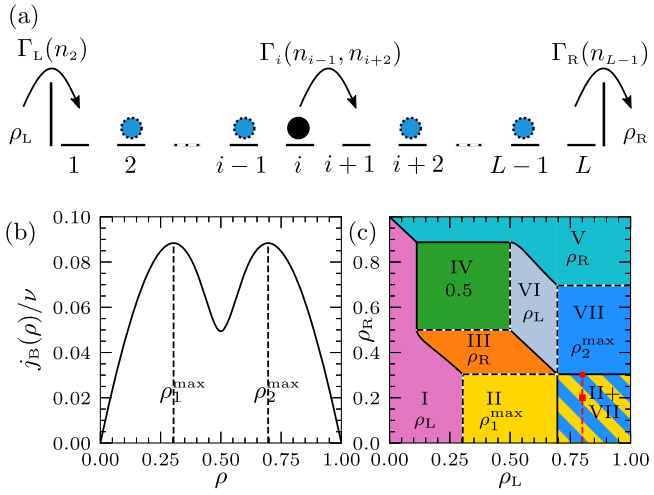

FIG. 1. (a) Illustration of the open TASEP with repulsive nearest-neighbor interaction V: Particles are injected with rate $\Gamma_L(n_2)$ from the left particle reservoir, ejected with rate $\Gamma_R(n_{L-1})$ to the right reservoir, and perform unidirectional jumps with rates $\Gamma_i(n_{i-1}, n_{i+2})$ (3) inside the system. (b) Current-density relation for $V = 2V_c = 4\ln(3)$ in the closed TASEP. (c) Nonequilibrium phase diagram following from (b) by applying the extremal current principle (1). In the yellow-blue shaded square the two maximum current phases II and VII coexist. The red square, circle, and line in this area mark reservoir densities, for which DW dynamics were simulated.

Here, ν is an attempt frequency and V the repulsive nearest-neighbor interaction in units of the thermal energy; n_i are occupation numbers, i.e., $n_i = 1$ if site i is occupied and $n_i = 0$ otherwise. We use ν^{-1} and the lattice constant as time and length units, respectively. The particle injection and ejection rates at the boundaries are bulk adapted [40,48]. Further details of the model are given in the Supplemental Material (SM) [49].

Above a critical value $V_c = 2\ln 3$, the bulk current-density relation $j_B(\rho)$ has a double hump structure, where $\rho = \langle n_i \rangle$ with $\langle \cdots \rangle$ the average in the NESS. The relation is known exactly [40,48] and shown in Fig. 1(b) for $V = 2V_c$. It has maxima at $\rho_1^{\max} = (1 - [3 - \sqrt{8e^V/(e^V - 1)}]^{1/2})/2 \cong 0.304$ and $\rho_2^{\max} = 1 - \rho_1^{\max} \cong 0.696$. Applying the extremal current principle (1) yields the phase diagram in Fig. 1(c). In the whole yellow-blue shaded square $\{(\rho_L, \rho_R) | \rho_2^{\max} < \rho_L < 1, 0 < \rho_R < \rho_1^{\max}\}$ at the lower right corner of the phase diagram, the two maximal current phases II and VII with $\rho = \rho_1^{\max}$ and $\rho_2^{\max}$ coexist in the open system. The phases are visible on a microscopic level by plotting particle trajectories, see SM.

Figures 2(a)–2(c) show representative density profiles of the coexisting phases at randomly chosen times in the NESS for different L and different reservoir densities (ρ_L, ρ_R) in the coexistence region II + VII. These profiles were determined from kinetic Monte Carlo (KMC) simulations by averaging the occupation numbers in a time window $\Delta t = 5 \times 10^4$. They decay from $\rho_2^{\max}$ to $\rho_1^{\max}$. Within the interval Δt, the DW occurs at different random positions, causing the profile to decay over a region larger than the intrinsic width ξ of the DW. Stationary profiles obtained from averaging over long times are represented by the thick blue lines in Figs. 2(a)–2(c). Videos of time-dependent density profiles are provided in the SM.

In Figs. 2(a) and 2(b), the system size $L = 500$ is the same, but the reservoir densities are different, with (a) $(\rho_L, \rho_R) = (0.8, 0.3016)$ very close to the boundary to phase VII [see Fig. 1(c)], and (b) $(\rho_L, \rho_R) = (0.8, 0.2)$ on the "symmetry line" $\rho_R = 1 - \rho_L$. While the mean position of the DW is close to the system's center in (b), it is shifted to the right in (a). In Fig. 2(c) the reservoir densities are the same as in Fig. 2(b), but the system size is eight times larger, $L = 4 \times 10^3$. For the larger system size in (c), the position fluctuations of the DW relative to the system size become smaller.

To quantify these effects, we have determined the instantaneous DW position by adding $N_g = 40$ ghost particles to the system, which neither interact with themselves nor affect the stochastic dynamics of the regular

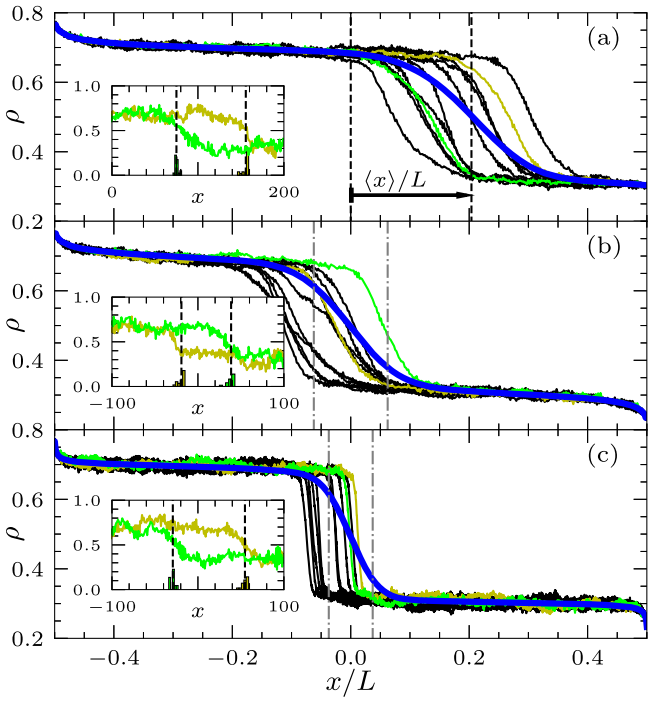

FIG. 2. Simulated density profiles in the coexistence region II + VII at randomly selected times (thin solid lines) for (a) $(\rho_L,\rho_R)=(0.8,0.3016)$ and $L=500$, (b) $(\rho_L,\rho_R)=(0.8,0.2)$ and $L=500$, and (c) $(\rho_L,\rho_R)=(0.8,0.2)$ and $L=4000$. The thick blue lines mark the long-time averaged densities. The dashed vertical lines in (a) indicate the displacement $\langle x\rangle$ of the mean DW position from the center. The dash-dotted vertical lines in (b) and (c) indicate the standard deviation $\pm w_{\rm sat}/L$ of the saturated DW position fluctuations around the center. The insets show two short-time averages of the fluctuating particle density (noisy green and olive curves), as well as histograms of the distribution of ghost particle positions. Their mean value marks the microscopic position of the DW (dashed vertical lines).

particles. After each jump of a regular particle, 50% of the ghost particles are randomly selected. If a selected ghost particle is on a site occupied (not occupied) by a regular particle it is moved one site to the right (left). Because of these dynamics, the ghost particles accumulate at the DW position, i.e., its instantaneous position $x(t)$ is accurately determined by the mean of the ghost particle positions y_j,

$$x(t)=\frac{1}{N_g}\sum_{j=1}^{N_g} y_j(t). \tag{4}$$

We set $y_j=i-(L+1)/2$ for ghost particle j at site i, giving $x(t)=0$ if the DW is at the system's center.

Histograms of ghost particle positions are shown in the insets of Figs. 2(a)–2(c), together with density profiles of the regular particles obtained from averages in shorter time windows $10^{-2}\Delta t$, in which the DW movement can be neglected. The standard deviation of the ghost particle positions is a measure of the DW's intrinsic width $\xi\simeq 4$, demonstrating that the DW is microscopically sharp. This is reminiscent of the microscopic sharpness of a shock discontinuity in the open ASEP [43,52,53]. In videos provided in the SM, we show the stochastic change of density profiles in time together with the coupled motion of the ghost particle cloud.

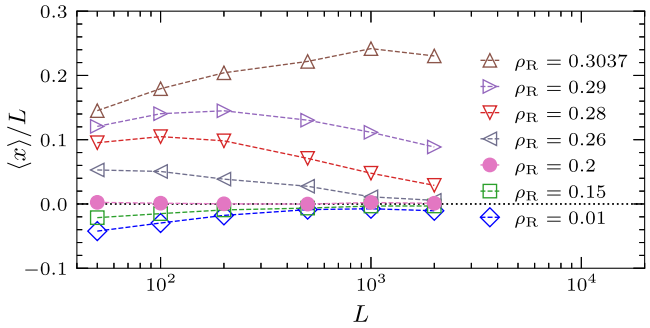

FIG. 3. Mean DW position $\langle x\rangle$ as a function of L for fixed $\rho_L=0.8$ and various ρ_R corresponding to points on the red dashed line shown in the coexisting region II + VII in Fig. 1(c). For large L, $\langle x\rangle\to 0$, demonstrating that the displacement $\langle x\rangle/L$ in Fig. 2(a) is a finite size effect.

Figure 3 shows the stationary mean DW position $\langle x\rangle$ as a function of the system size L for reservoir densities $(\rho_L=0.8,\rho_R)$ along the red line indicated in the coexistence region II + VII of the phase diagram in Fig. 1(c). For small L, $\langle x\rangle$ is displaced from the center of the system, except for $\rho_R=1-\rho_L=0.2$. When ρ_R approaches $\rho_1^{\rm max}$, the displacement increases at fixed L. This can be explained by the fact that when ρ_R crosses $\rho_1^{\rm max}$ (at fixed $\rho_L=0.8$), the NESS becomes the maximal current phase VII with $\rho_B=\rho_2^{\rm max}$. Phase II is thus increasingly expelled from the system as ρ_R approaches $\rho_1^{\rm max}$. However, when increasing L at fixed (ρ_L,ρ_R), the displacement of the mean DW position from the center decreases and approaches zero for large L. This means that the displacement indicated in Fig. 2(a) is a finite-size effect.

We now analyze the stationary fluctuations of the DW position for $(\rho_L,\rho_R)=(0.8,0.2)$, where $\langle x\rangle=0$ for all L. To this end we define the width of these fluctuations by the standard deviation of the displacement of the instantaneous DW position $x(t)$ from the mean position $\bar{x}(t)=\sum_{t'=0}^{t}x(t')/(t+1)$ after time t,

$$w(t,L)=\left\langle\frac{1}{(t+1)}\sum_{t'=0}^{t}[x(t')-\bar{x}(t')]^2\right\rangle^{1/2}. \tag{5}$$

Figure 4(a) shows $w(t,L)$ as a function of time for various L. At small t, $w(t,L)\sim t^{1/3}$ independent of L, while for large times, w saturates at a value $w_{\rm sat}\sim L^{3/4}$. When plotting the data in scaled form according to Eq. (2), they collapse onto one master curve, see Fig. 4(b).

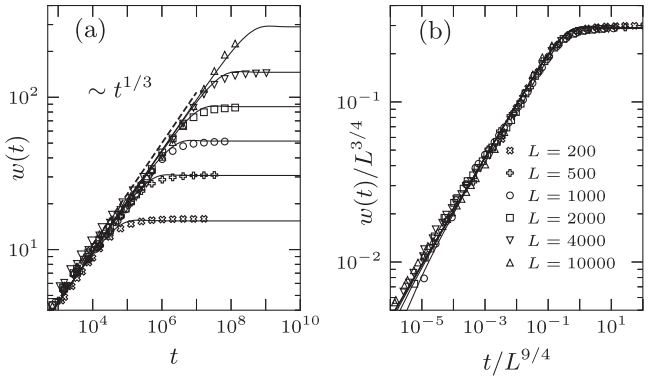

FIG. 4. (a) Width $w(t, L)$ of DW position fluctuations [see Eq. (5)] as a function of time for various system sizes L. (b) Scaled width $w(t, L)/L^{3/4}$ as a function of scaled time $t/L^{9/4}$ demonstrating the scaling law (2). The legend in (b) applies to (a) also. Solid lines indicate the results from the Ornstein-Uhlenbeck process given by Eq. (8) with parameters $\kappa_0 = 1.133$ and $C_\infty = 0.0225$.

We now provide a description of the stochastic domain wall motion based on theories for kinematic waves [54], and for current correlations and density profiles in the NESS of DLGs [48,55]. As a consequence of particle number conservation, the velocity of a shock front is $v = [j(\rho_2) - j(\rho_1)]/(\rho_2 - \rho_1)$, where ρ_2 (ρ_1) are the particle densities before (after) the shock front. Applying this law to particle densities $\rho_\pm(x) \simeq \rho(x \pm \xi)$ and fluctuating currents $j_B(\rho_\pm(x)) + \delta j_\pm(t)$ right and left of the DW, we can write

$$\frac{\mathrm{d}x}{\mathrm{d}t} = \frac{j_B(\rho_-(x)) - j_B(\rho_+(x)) + \delta j(t)}{\rho_-(x) - \rho_+(x)} \simeq \frac{\delta j(t)}{\rho_2^{\max} - \rho_1^{\max}}. \quad (6)$$

Here we have set $\rho_-(x) \simeq \rho_2^{\max}$, $\rho_+(x) \simeq \rho_1^{\max}$, and $\delta j(t) = \delta j_-(t) - \delta j_+(t)$.

The scaling of correlation functions between occupation numbers in the NESS of DLGs falls into the KPZ universality class, which implies that current fluctuations are long-range anticorrelated. Their autocorrelation function decays as

$$C(t) = \langle \delta j(t) \delta j(0) \rangle \sim -t^{-4/3} \quad (7)$$

at long times, and the integral over $C(t)$ vanishes [55]. These two properties of $C(t)$ lead to the subdiffusive $t^{1/3}$ scaling of $w(t, L)$, see Eq. (S11) in the SM.

As for the weak pinning of the DW, we argue that it is caused by the tendency of the density profiles left and right from the DW to match profiles of the corresponding maximal current phases. The functional form of these matching profiles is universal and decays as a power law $\sim 1/\sqrt{l}$ with the distance l from the boundary [36,48]. Thus, close to $x = 0$ the mean densities left and right of the DW are slightly different from $\rho_2^{\max}$ and $\rho_1^{\max}$, and their gradients give rise to a restoring force of the DW position towards $x = 0$. As these gradients are very small and decrease with L, a linear approximation $\delta\rho(x) = \delta\rho'(0)x$ should be appropriate. This suggests that the restoring force is linear with a strength decreasing with L. We hence write

$$\frac{\mathrm{d}x}{\mathrm{d}t} = -\kappa(L)x + \eta(t), \quad (8)$$

where $\kappa(L) \to 0$ for $L \to \infty$, and $\eta(t)$ is a stationary Gaussian process with zero mean and autocorrelation function $C(t)$ with $\int_0^\infty \mathrm{d}t C(t) = 0$ and asymptotic behavior $C(t) \sim -C_\infty (rt)^{-4/3}$ for $t \to \infty$; $C_\infty > 0$ is a constant and r^{-1} a microscopic timescale (e.g., the inverse attempt frequency $\nu^{-1} = 1$ in the TASEP model).

Equation (8) describes an Ornstein-Uhlenbeck process with long-range anticorrelated noise. As shown in the SM, it holds $w_{\mathrm{sat}}^2 = \tilde{C}(\kappa)/\kappa$, where $\tilde{C}(\kappa)$ is the Laplace transform of $C(t)$, with the asymptotic behavior $\tilde{C}(\kappa) \sim \kappa^{1/3}$ for $\kappa \to 0$ [see Eqs. (S12) and (S13)]. Accordingly, $w_{\mathrm{sat}} \sim \kappa(L)^{-1/3}$. With $w_{\mathrm{sat}} \sim L^{3/4}$ from the simulations, we conclude

$$\kappa(L) \sim \kappa_0 L^{-9/4} \quad (9)$$

for large L, where $\kappa_0 > 0$ is a constant. This shows that the nonflatness of the density profiles in extremal current phases gives rise to the characteristic timescale $\kappa^{-1} \sim L^{9/4}$ in the scaling behavior of $w(t, L)$. A detailed analysis of Eq. (8) in the SM yields a scaling function $f(u)$, which behaves as $f(u) \sim 3C_\infty^{1/2} r^{-2/3} u^{1/3}$ for $u \ll 1$ and $f(u) \sim \mathrm{const} = [3\Gamma(\frac{2}{3})C_\infty]^{1/2} r^{-2/3} \kappa_0^{-1/3}$ for $u \gg 1$ [$\Gamma(.)$ is the Gamma function]. The simulated data can be well fitted by this model, see the solid lines in Fig. 4.

We have verified also the linear restoring force by determining the drift coefficient $D_1 = \langle [x(t+\tau) - x(t)] | x(t) = x \rangle / \tau$ in simulations, see SM. As the DW is well defined only on a coarse-grained timescale, we cannot take the limit $\tau \to 0$ and have analyzed D_1 for different τ [56]. For the Ornstein-Uhlenbeck process in Eq. (8), $D_1 = D_1(x, L; \tau) = -x(1 - e^{-\kappa\tau})/\tau$ with $\kappa = \kappa_0/L^{9/4}$. Our simulation results are in agreement with this prediction, but with a κ depending on τ, approaching a constant $\propto L^{-9/4}$ for large τ. This means that Eq. (8) does not provide a complete description of the DW dynamics. We believe that memory effects need to be included in the restoring process in Eq. (8).

In summary, we have shown for the TASEP with repulsive nearest-neighbor interaction that the DW separating extremal current phases is microscopically sharp and exhibits surprisingly rich stochastic dynamics. A subdiffusive growth of the variance of the DW position arises from anticorrelated current fluctuations. At large

times $t \gg \kappa(L)^{-1} \sim L^{9/4}$ the DW becomes weakly pinned in a region increasing sublinearly with the system size.

Because these phenomena occur on large time and length scales, they are independent of microscopic details and therefore expected to hold true in general for driven diffusive systems with short-range particle interactions. A necessary condition for coexistence of extremal current phases is a bulk current-density relation exhibiting local maxima (minima) of the same value, and no higher maximum (lower minimum) lying in between them. The DW dynamics between such phases reflect power law decays of current correlations and density profiles. Their investigation can thus be used as a dynamical probe for analyzing these pertinent features of driven diffusive systems.

We interpret the weak pinning by the tendency of the density profiles left and right of the DW to match their preferred shapes. On the macroscopic scale, i.e., by rescaling the lattice by $1/L$, the density profile has two constant segments of densities $\rho_2^{\max}$ and $\rho_1^{\max}$, respectively. The DW marking the transition point from $\rho_2^{\max}$ to $\rho_1^{\max}$ becomes sharp and corresponds to a so-called contact discontinuity [57]. In contrast to the microscopically well-understood shock discontinuities appearing in the ASEP on the coexistence line, see, e.g., [52,58–61], little is known about the microscopic structure of contact discontinuities in DLGs. Our findings constitute a first step towards their systematic exploration.

A puzzling question is how the dynamical exponent $9/4$ for the crossover time arises. It seems that the present understanding of dynamical critical phenomena in driven diffusion systems is not yet complete.

This work has been funded by the Deutsche Forschungsgemeinschaft (DFG, Project No. 355031190), by FCT/Portugal through CAMGSD, IST-ID, Projects No. UIDB/04459/2020 and No. UIDB/04459/2020, and by the FCT Grant No. 2022.09232.PTDC. We sincerely thank A. Zahra, V. Popkov, and the members of the DFG Research Unit FOR2692 for fruitful discussions.

*sschweers@uos.de
†david.locher@rwth-aachen.de
‡gschuetz04@yahoo.com
§maass@uos.de

[1] H. Spohn, *Large Scale Dynamics of Interacting Particles* (Springer-Verlag, Berlin, 1991).
[2] B. Schmittmann and R. K. P. Zia, Statistical mechanics of driven diffusive systems, in *Phase Transitions and Critical Phenomena*, edited by C. Domb and J. Lebowitz (Academic Press, London, 1995), Vol. 17.
[3] H. Spohn, The Kardar–Parisi–Zhang equation: A statistical physics perspective, in *Stochastic Processes and Random Matrices: Lecture Notes of the Les Houches Summer School: Volume 104, July 2015* (Oxford University Press, New York, 2017).
[4] J. Quastel and S. Sarkar, Convergence of exclusion processes and KPZ equation to the KPZ fixed point, J. Am. Math. Soc. **36**, 251 (2023).
[5] B. Derrida, An exactly soluble non-equilibrium system: The asymmetric simple exclusion process, Phys. Rep. **301**, 65 (1998).
[6] G. M. Schütz, Exactly solvable models for many-body systems far from equilibrium, in *Phase Transitions and Critical Phenomena*, edited by C. Domb and J. Lebowitz (Academic Press, London, 2001), Vol. 19, pp. 1–251.
[7] E. Frey, A. Parmeggiani, and T. Franosch, Collective phenomena in intracellular processes, Genome Inf. **15**, 46 (2004).
[8] R. A. Blythe and M. R. Evans, Nonequilibrium steady states of matrix-product form: A Solver's guide, J. Phys. A Math. Theor. **40**, R333 (2007).
[9] A. Schadschneider, D. Chowdhury, and K. Nishinari, *Stochastic Transport in Complex Systems: From Molecules to Vehicles*, 3rd ed. (Elsevier Science, Amsterdam, 2010), 10.1016/C2009-0-16900-3.
[10] T. Kriecherbauer and J. Krug, A pedestrian's view on interacting particle systems, KPZ universality and random matrices, J. Phys. A Math. Gen. **43**, 403001 (2010).
[11] T. Chou, K. Mallick, and R. K. P. Zia, Non-equilibrium statistical mechanics: From a paradigmatic model to biological transport, Rep. Prog. Phys. **74**, 116601 (2011).
[12] V. Popkov, A. Schadschneider, J. Schmidt, and G. M. Schütz, Fibonacci family of dynamical universality classes, Proc. Natl. Acad. Sci. U.S.A. **112**, 12645 (2015).
[13] K. Mallick, The exclusion process: A paradigm for non-equilibrium behaviour, Physica (Amsterdam) **418A**, 17 (2015).
[14] X. Fang, K. Kruse, T. Lu, and J. Wang, Nonequilibrium physics in biology, Rev. Mod. Phys. **91**, 045004 (2019).
[15] V. Kukla, J. Kornatowski, D. Demuth, I. Girnus, H. Pfeifer, L. V. C. Rees, S. Schunk, K. K. Unger, and J. Kärger, NMR studies of single-file diffusion in unidimensional channel zeolites, Science **272**, 702 (1996).
[16] Q.-H. Wei, C. Bechinger, and P. Leiderer, Single-file diffusion of colloids in one-dimensional channels, Science **287**, 625 (2000).
[17] B. Hille, *Ion Channels of Excitable Membranes*, 3rd ed. (Sinauer, Sunderland, Mass, 2001).
[18] C. T. MacDonald, J. H. Gibbs, and A. C. Pipkin, Kinetics of biopolymerization on nucleic acid templates, Biopolymers **6**, 1 (1968).
[19] L. Ciandrini, I. Stansfield, and M. C. Romano, Role of the particle's stepping cycle in an asymmetric exclusion process: A model of mRNA translation, Phys. Rev. E **81**, 051904 (2010).
[20] S. Klumpp and T. Hwa, Stochasticity and traffic jams in the transcription of ribosomal RNA: Intriguing role of termination and antitermination, Proc. Natl. Acad. Sci. U.S.A. **105**, 18159 (2008).
[21] R. K. P. Zia, J. J. Dong, and B. Schmittmann, Modeling translation in protein synthesis with tasep: A tutorial and recent developments, J. Stat. Phys. **144**, 405 (2011).
[22] D. D. Erdmann-Pham, K. Dao Duc, and Y. S. Song, The key parameters that govern translation efficiency, Cell Syst. **10**, 183 (2020).

[23] J. Keisers and J. Krug, Exclusion model of mRNA translation with collision-induced ribosome drop-off, J. Phys. A Math. Theor. **56**, 385601 (2023).
[24] R. Lipowsky, J. Beeg, R. Dimova, S. Klumpp, and M. J. Müller, Cooperative behavior of molecular motors: Cargo transport and traffic phenomena, Physica (Amsterdam) **42E**, 649 (2010).
[25] D. Chowdhury, Stochastic mechano-chemical kinetics of molecular motors: A multidisciplinary enterprise from a physicist's perspective, Phys. Rep. **529**, 1 (2013).
[26] A. B. Kolomeisky, *Motor Proteins and Molecular Motors* (CRC Press, Boca Raton, 2015), 10.1201/b18426.
[27] A. Jindal, A. B. Kolomeisky, and A. K. Gupta, The role of dynamic defects in transport of interacting molecular motors, J. Stat. Mech. (2020) 043206.
[28] T. Halpin-Healy and K. A. Takeuchi, A KPZ cocktail-shaken, not stirred..., J. Stat. Phys. **160**, 794 (2015).
[29] J. Krug, Origins of scale invariance in growth processes, Adv. Phys. **46**, 139 (1997).
[30] K. A. Takeuchi and M. Sano, Universal fluctuations of growing interfaces: Evidence in turbulent liquid crystals, Phys. Rev. Lett. **104**, 230601 (2010).
[31] K. Nagel and M. Schreckenberg, A cellular automaton model for freeway traffic, J. Phys. I (France) **2**, 2221 (1992).
[32] D. Chowdhury, L. Santen, and A. Schadschneider, Statistical physics of vehicular traffic and some related systems, Phys. Rep. **329**, 199 (2000).
[33] D. Helbing, Traffic and related self-driven many-particle systems, Rev. Mod. Phys. **73**, 1067 (2001).
[34] S. Maerivoet and B. De Moor, Cellular automata models of road traffic, Phys. Rep. **419**, 1 (2005).
[35] A. Gupta, B. Pal, A. Jindal, N. Bhatia, and A. K. Gupta, Modelling of transport processes: Theory and simulations, MethodsX **10**, 101966 (2023).
[36] J. Krug, Boundary-induced phase transitions in driven diffusive systems, Phys. Rev. Lett. **67**, 1882 (1991).
[37] Y. Kafri, E. Levine, D. Mukamel, G. M. Schütz, and R. D. Willmann, Phase-separation transition in one-dimensional driven models, Phys. Rev. E **68**, 035101(R) (2003).
[38] T. Antal and G. M. Schütz, Asymmetric exclusion process with next-nearest-neighbor interaction: Some comments on traffic flow and a nonequilibrium reentrance transition, Phys. Rev. E **62**, 83 (2000).
[39] M. Dierl, P. Maass, and M. Einax, Classical driven transport in open systems with particle interactions and general couplings to reservoirs, Phys. Rev. Lett. **108**, 060603 (2012).
[40] M. Dierl, M. Einax, and P. Maass, One-dimensional transport of interacting particles: Currents, density profiles, phase diagrams, and symmetries, Phys. Rev. E **87**, 062126 (2013).
[41] V. Popkov and G. M. Schütz, Steady-state selection in driven diffusive systems with open boundaries, Europhys. Lett. **48**, 257 (1999).
[42] A. B. Kolomeisky, G. M. Schütz, E. B. Kolomeisky, and J. P. Straley, Phase diagram of one-dimensional driven lattice gases with open boundaries, J. Phys. A **31**, 6911 (1998).
[43] A. Parmeggiani, T. Franosch, and E. Frey, Phase coexistence in driven one-dimensional transport, Phys. Rev. Lett. **90**, 086601 (2003).
[44] P. Roy, A. K. Chandra, and A. Basu, Pinned or moving: States of a single shock in a ring, Phys. Rev. E **102**, 012105 (2020).
[45] G. Schütz and E. Domany, Phase transitions in an exactly soluble one-dimensional exclusion process, J. Stat. Phys. **72**, 277 (1993).
[46] B. Derrida, S. A. Janowsky, J. L. Lebowitz, and E. R. Speer, Exact solution of the totally asymmetric simple exclusion process: Shock profiles, J. Stat. Phys. **73**, 813 (1993).
[47] S. Katz, J. L. Lebowitz, and H. Spohn, Nonequilibrium steady states of stochastic lattice gas models of fast ionic conductors, J. Stat. Phys. **34**, 497 (1984).
[48] J. S. Hager, J. Krug, V. Popkov, and G. M. Schütz, Minimal current phase and universal boundary layers in driven diffusive systems, Phys. Rev. E **63**, 056110 (2001).
[49] See Supplemental Material at http://link.aps.org/supplemental/10.1103/PhysRevLett.132.167101 for details of the model and simulations, a representation of the DW based on particle trajectories, the derivation of the DW width following from Eq. (8), results for the drift coefficient, and videos illustrating the DW motion. This includes Refs. [50,51].
[50] D. T. Gillespie, Monte Carlo simulation of random walks with residence time dependent transition probability rates, J. Comput. Phys. **28**, 395 (1978).
[51] V. Holubec, P. Chvosta, M. Einax, and P. Maass, Attempt time Monte Carlo: An alternative for simulation of stochastic jump processes with time-dependent transition rates, Europhys. Lett. **93**, 40003 (2011).
[52] K. Krebs, F. H. Jafarpour, and G. M. Schütz, Microscopic structure of travelling wave solutions in a class of stochastic interacting particle systems, New J. Phys. **5**, 145 (2003).
[53] G. M. Schütz, A reverse duality for the ASEP with open boundaries, J. Phys. A **56**, 274001 (2023).
[54] M. J. Lighthill and G. B. Whitham, On kinematic waves II. A theory of traffic flow on long crowded roads, Proc. R. Soc. A **229**, 317 (1955).
[55] P. L. Ferrari and H. Spohn, On time correlations for KPZ growth in one dimension, SIGMA **12**, 074 (2016).
[56] C. Anteneodo and S. M. D. Queirós, Low-sampling-rate Kramers-Moyal coefficients, Phys. Rev. E **82**, 041122 (2010).
[57] A. Bressan, Hyperbolic systems of conservation laws, Rev. Mat. Complutense **12**, 135 (1999), http://eudml.org/doc/44436.
[58] P. A. Ferrari, C. Kipnis, and E. Saada, Microscopic structure of travelling waves in the asymmetric simple exclusion process, Ann. Probab. **19**, 226 (1991).
[59] B. Derrida, J. L. Lebowitz, E. R. Speer, and E. R. Speer, Shock profiles for the asymmetric simple exclusion process in one dimension, J. Stat. Phys. **89**, 135 (1997).
[60] M. Balázs, G. Farkas, P. Kovács, and A. Rákos, Random walk of second class particles in product shock measures, J. Stat. Phys. **139**, 252 (2010).
[61] V. Belitsky and G. M. Schütz, Microscopic structure of shocks and antishocks in the ASEP conditioned on low current, J. Stat. Phys. **152**, 93 (2013).